UCRL-52556

NUMERICAL SIMULATION OF MATERIAL TRANSPORT IN A REGIONAL GROUND-WATER FLOW SYSTEM

T. G. Naymik
L. D. Thorson

December 31, 1978

This work was supported by the U.S. Nuclear Regulatory Commission under Interagency Agreement DOE 40-550-75 with the U.S. Department of Energy.

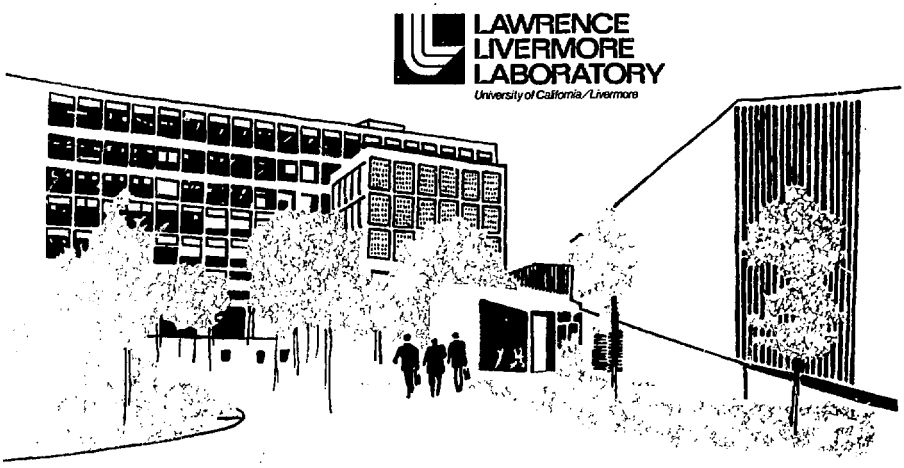

LAWRENCE LIVERMORE LABORATORY
University of California Livermore California 94550

UCRL-52556

NUMERICAL SIMULATION OF MATERIAL TRANSPORT IN A REGIONAL GROUND-WATER FLOW SYSTEM

E. G. Naymik
E. D. Thorson

MS. date: December 31, 1978

CONTENTS

FIGURES

TABLES

ABSTRACT

A numerical model of a regional ground-water flow system (not site specific) was coupled with a material transport model in order to study the influence of porosity and distribution coefficients in bedded media. The effects on model performance were discerned from long-term material transport simulations. Model performance was based on initial breakthrough time, average breakthrough time, and the standard deviation of the breakthrough curve at a discharge surface. Large differences in model performance occurred when the distribution coefficient was changed less than an order of magnitude, while small differences resulted from changing porosity several orders of magnitude.

INTRODUCTION

Numerical models have value in predicting the effects of processes that occur over long periods of time. Ground-water and material transport codes can be used to study the movement of dissolved constituents in regional ground-water flow regimes.[1,2] By varying parameters and making multiple simulations, the effects of transport phenomena acting within a ground-water system can be singled out. In this paper, we varied porosity and distribution coefficient in long-term simulations of material transport in ground water.

GOVERNING EQUATIONS AND ASSUMPTIONS

The numerical calculations are done in a two-step process. First, the velocity field is calculated with a hydrology code originated by Taylor and Brown.[3,4] These velocities become input to a material transport code that provides concentration as a function of space and time. This code is a heavily modified version of a code written by Dugid and Reeves.[5,6]

The velocity field is calculated with a steady-state finite element code. The code allows for nonhomogeneous and nonisotropic layered material. Fluid flow is governed by Darcy's Law which can be written as

$$\bar{q} = -\bar{\bar{K}} \nabla\Phi \quad , \tag{1}$$

where $\bar{q}$ is the specific flux vector, $\bar{\bar{K}} = \bar{\bar{k}}\gamma/\mu$ is hydraulic conductivity, and $\Phi = P/\gamma + z$ is the piezometric head. Additional notation and definitions can be found in Table 1.

The steady-state head distribution is found using Darcy's Law in the continuity equation,

$$\nabla \cdot (\rho\bar{q}) = 0 \quad , \tag{2}$$

and applying appropriate boundary conditions. For our problems, three different boundary conditions are used. Along the bottom and most of the sides of the modeled basin, we use a no-flow condition. A small segment at one end is designated as a recharge boundary. This recharge serves as the driving force for ground-water flow in the basin. Along the top, a free surface condition is used. These conditions can be written as

$\bar{n} \cdot \bar{q} = 0$	no flow	
$\bar{n} \cdot \bar{q} = \alpha$	recharge	(3)
$P = 0$	along the free surface	

TABLE 1. Notation.

$\bar{q}$ = specific flux vector (Darcy velocity)

$\bar{\bar{K}}$ = $\bar{\bar{k}}\gamma/\mu$ = hydraulic conductivity tensor

$\bar{\bar{k}}$ = permeability tensor

g = gravity

P = pressure

z = height above a horizontal datum

n = porosity

$\bar{v}$ = true velocity

D_{ij} = hydrodynamic dispersion

c = concentration of the dissolved constituent

$R_d = 1 + \frac{\rho K_d}{n}$ = retardation factor

a_T = transverse dispersivity

a_L = longitudinal dispersivity

a_m = molecular diffusion

K_d = distribution coefficient

γ = ρg

ρ = density

Φ = $P/\gamma + z$ piezometric head

μ = viscosity

λ = radioactive decay constant

τ = tortuosity

where n is the normal to the surface and α is a constant that specifies the amount of fluid added by recharge.

The free surface is the interface between the unsaturated and saturated zones, i.e., the water table, which occurs at or below the land surface. With changes in recharge, this surface can be made to move up and down. For our purposes, it is assumed that the free surface and land surface coincide. This assumption is reasonable because of the thickness of the basin compared with the small distance from the land surface to the water table.

Given the head distribution, a true velocity is calculated and used as input to the transport code. The relationship between the Darcy velocity and the true velocity is

$$\bar{v} = \frac{\bar{q}}{n} \quad . \tag{4}$$

To calculate the movement of the dissolved constituent, we solve

$$\nabla \cdot (\bar{D} \cdot \nabla c) - \nabla \cdot (\bar{v} c) + \lambda R_d c = R_d \frac{\partial c}{\partial t} \quad , \tag{5}$$

where D is the hydrodynamic dispersion tensor, which can be written as

$$D_{ij} = a_T v \delta_{ij} + (a_L - a_T) \frac{v_i v_j}{v} + a_m \tau \delta_{ij} \tag{6}$$

and

$$v = \sqrt{v_i^2 + v_j^2}$$

The derivation of equations 5 and 6 can be found in Bear.[7]

In equation (5), R_d, the retardation factor, is used. The calculations, however, vary K_d, the distribution coefficient. The relationship between the two is

$$R_d = 1 + \frac{\rho K_d}{n} \quad . \tag{7}$$

Of prime concern here is the time it takes for a contaminant to travel from the repository to an outlet boundary, the travel time. This can be found by graphing the concentration at the boundary as a function of time. In this manner, the initial breakthrough time and the time of maximum concentration can easily be determined. As can be seen from equation (5), the contaminant moves with the true velocity. The effect of $\bar{\bar{D}}$ is to smear the contaminant front around this position. The effect of porosity is thus made clear, true velocity being inversely proportional to porosity, as can be seen from equation (4). Equation (5) is solved in vertical cross section using a Galerkin finite-element approach with isoparametric elements.

In our model, we have made several assumptions. The most important is that we can represent a nuclear waste repository in geologic media as a "point source" in vertical cross section. This assumption should give us conservative results, in that concentrations will be higher at the outlet than what would be expected in a three-dimensional model.

We also assume an isothermal situation. This presents no difficulty except close to a repository. The effect of high temperatures near the repository is to lower the water viscosity and hence increase the hydraulic conductivity. This influences the flow field locally. Additionally, we assume that the presence of a repository has no effect on the flow field. In reality, it takes some time to fill the repository and to reestablish the flow field before there can be a release of nuclides into the ground water. Our problem begins with the initial release from the repository.

We also assume that trace amounts of nuclides are present. Therefore, density variations may be neglected. Again the error induced would be local to the repository and should not influence the flow field over a large area.

The major assumption involved with the hydrologic calculations has to do with the same boundary conditions persisting over long periods of time, i.e., steady state. The effect of a prolonged drought would be to slow down the movement of the nuclides. On the other hand, increased rainfall would have the opposite effect. This concept is under investigation at present on the basin-wide scale.

DESCRIPTION OF THE BASIN

A generic model was developed for a large sedimentary basin (Fig. 1). The dimensions of the basin are 160 km by 255 km. A ground-water divide is assumed at the basin perimeter (point A), and ground-water discharge is assumed at a river (point B). A vertical plane of symmetry is assumed below the river at point B. The elevation at point A is defined as 1308 m to simulate the marginal upland of the basin. There are 560 m of relief between point A and point B. Four topographic slope changes are defined on the 80-km cross section. Two slope changes in the upland region simulate possible erosional topography in the lower layers that crop out at the margin. The long, gentle slope present on layer 1 represents overlapping apron deposits between the uplands and the river. A large flat-lying flood plain associated with the river is the fourth topographic feature.

The stratigraphy is divided into five vertical hydrologic units, all of which have fairly low hydraulic conductivities (Fig. 2). The succession of units down from the surface is: (1) an aquifer with a hydraulic conductivity of 200 m/y, and thickness of 170 m that outcrops on the horizontal axis between 21 km and 80 km; (2) an aquitard with K = 20 m/y, 136 m thick, that outcrops between 15 km and 21 km; (3) an aquiclude with K = 1 m/y, 170 m thick, that outcrops between 12 km and 15 km; (4) an aquitard with K = 20 m/y, 136 m thick, that outcrops between 8 km and 12 km; and (5) an aquifer with K = 200 m/y, 136 m thick, that outcrops between 0 km and 8 km.

The hydrologic setting of the basin (Fig. 3) contains three key features: (1) at line AE, a regional ground-water divide exists; (2) along line EC, the basin ground-water streamlines diverge from the regional flow pattern; and (3) line CD designates a symmetry plane for discharge in the basin flow regime. The basin is modeled most efficiently using these assumptions. Half of the basin is modeled because of the symmetry at the discharge region. The discharge region is treated as a broad flood plain. The ground-water divide is used as the vertical upland boundary, and the divergence between basin and

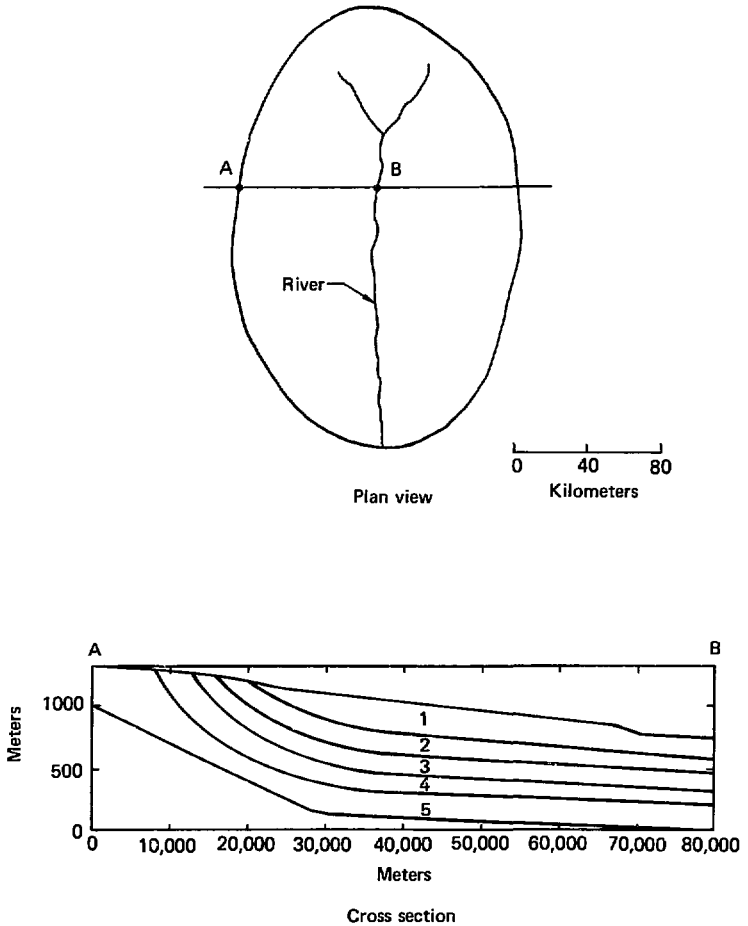

FIG. 1. Plan view of the generic sedimentary basin and cross section of half of the basin, AB.

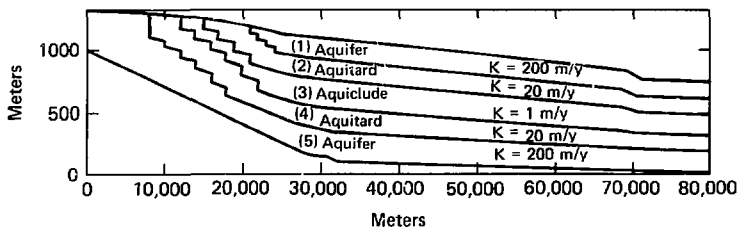

FIG. 2. Zones of hydraulic conductivities used in the model.

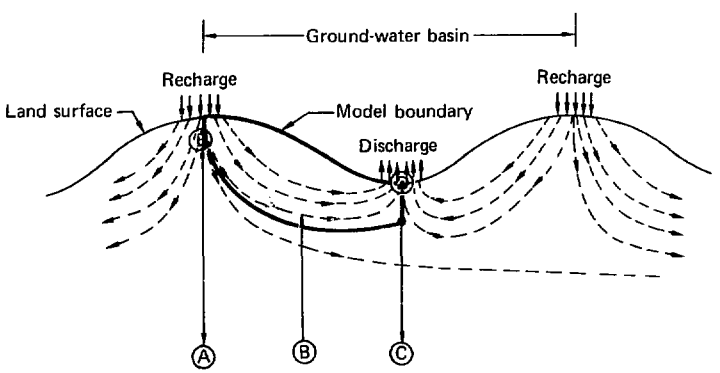

FIG. 3. Idealized hydrologic setting of the model (cross section). Line AE is the regional ground-water divide, point B is divergence of regional and basin flow, and line C-D is symmetry plane for basin discharge.

regional flow is used as the lower boundary. The resulting general basin flow pattern through the designated hydrologic units is shown with arrows (Fig. 4).

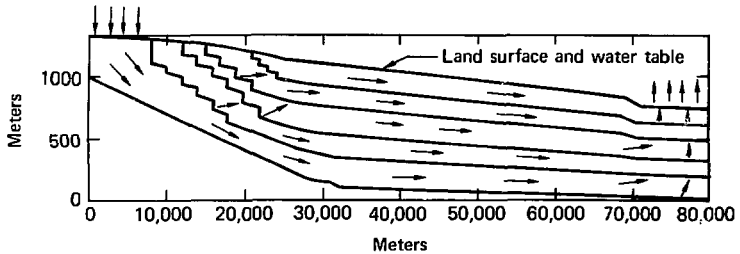

FIG. 4. Generalized ground-water flow pattern shown by arrows.

The numerical finite-element model is designed to simulate the steady flow of ground water through the basin. (The model contains 1656 nodal points defining 1562 elements.) The recharge region is treated as a distributed inflow boundary (Fig. 5). The ground-water divide, the divergence between basin and regional flow, and the symmetry plane at the discharge region are modeled as no-flow boundaries. The discharge region (flood plain) is simulated by a surface where hydraulic head equals elevation. Hydrologically, the boundary could simulate ground-water evaporation at or near the surface; transpiration by phreatophytes living on the flood plain; evaporation from lakes, pools, rivers, etc.; overland flow in streams and rivers; and similar processes. The water table is assumed to be coincident with land surface.

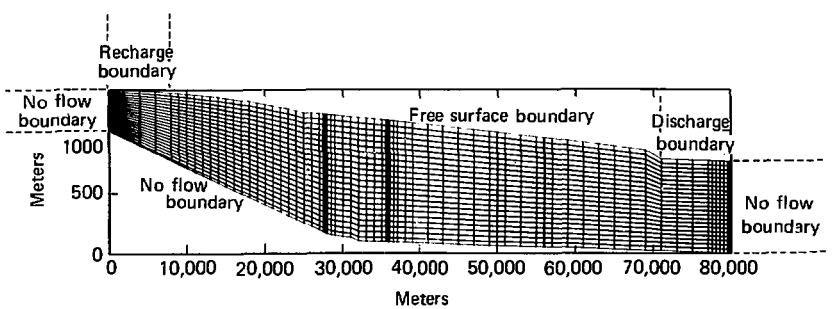

FIG. 5. Finite element mesh and model boundary conditions.

This is reasonable because in large areas where the relief is not great, the water table conforms to but is slightly below the land surface.

Figure 6 shows the equipotential lines within the basin cross section. At the recharge end (0 km to 8 km), the potential difference is very slight in comparison with the remainder of the basin. The highest flow potential appears in the (18 km to 24 km) interval where artesian conditions exist in the lower hydrologic units. Four intervals of the model cross section were chosen to demonstrate the equipotential surface in detail (Fig. 7). The recharge region (Fig. 7a) is characterized by a low potential and a slightly downward flow direction. The recharge is directly into the lower aquifer in which artesian conditions form at the major change in topographic slope of the basin, 24 km to 29 km (Fig. 7b). Flow is slightly upward in the lower aquifer and upper and lower aquitards, with a dominant upward flow direction in the aquiclude. No artesian head is present in the units further downgradient (Fig. 7c). Flow in the full thickness of the cross section follows the water table gradient to about 72 km (Fig. 7d) where, because of no-flow boundaries and increased head, the flow is turned up to the discharge surface. Velocity vector plots associated with Figs. 7a, 7b, 7c, and 7d appear in Figs. 8a, 8b, 8c, and 8d. Note the vertical scale exaggeration in Figs. 6, 7, and 8.

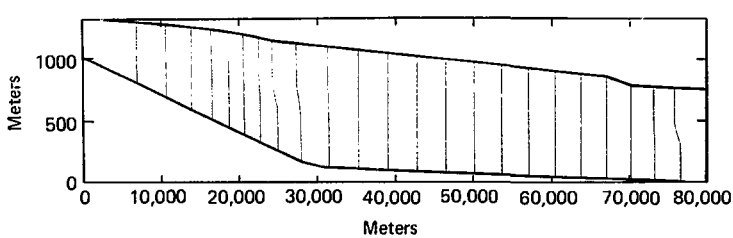

FIG. 6. Equipotential lines generated from model calculations.

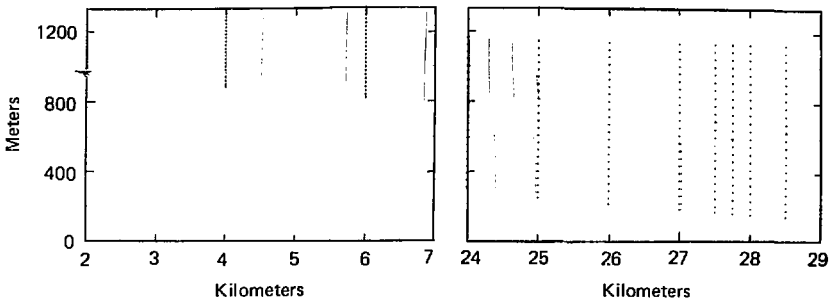

(a) Recharge region. Model interval 2 km to 7 km.

(b) Artesian conditions. Model interval 24 km to 29 km.

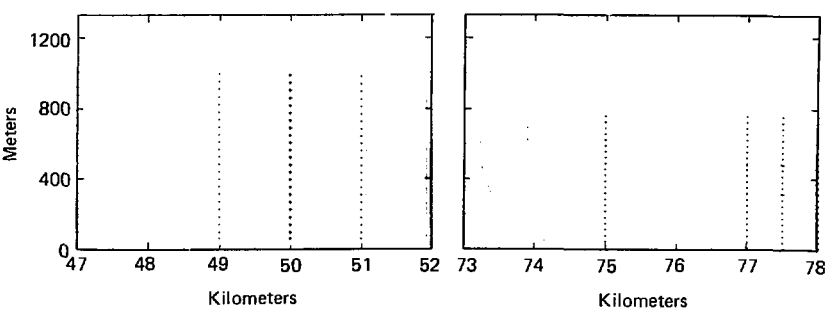

(c) Downgradient flow. Model interval 47 km to 52 km.

(d) Discharge region. Model interval 73 km to 78 km.

FIG. 7. Equipotential plots of four model intervals that illustrate the important areas of Fig. 6 in detail. The equipotential interval is the same for each of the four sections. The nodes (+) are also shown.

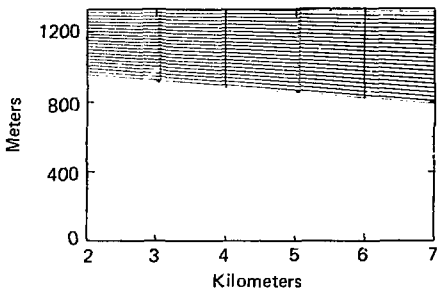

(a) Recharge region. Model interval 2 km to 7 km.

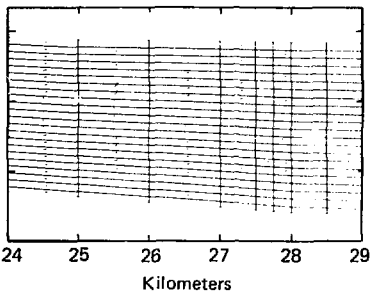

(b) Artesian conditions. Model interval 24 km to 29 km.

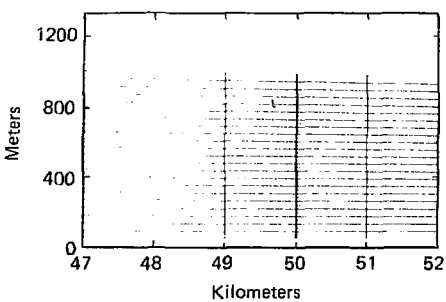

(c) Downgradient flow. Model interval 47 km to 52 km.

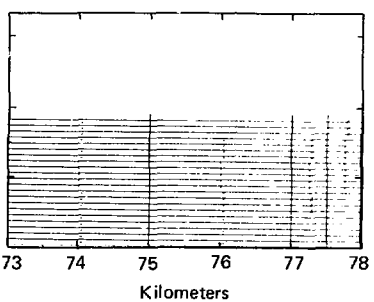

(d) Discharge region. Model interval 73 km to 78 km.

FIG. 8. Velocity vector plots of four model intervals that illustrate the areas of Fig. 6 in detail.

MATERIAL TRANSPORT

Given a velocity field, as calculated from the hydrologic model, only the transport properties of the media and the location of the material source remain to influence the contaminant transfer performance of the model. Model performance is based on average breakthrough time and the standard deviation of the breakthrough curve at the discharge surface. In the cases of incomplete breakthrough curves, comparisons are based on the initial breakthrough time.

DESCRIPTION OF BASIN TRANSPORT PROPERTIES

The basin cross section can represent a variety of stratified media by virtue of the mesh design and the flexibility of the input parameters that control material transport. As a starting point, we selected the parameter values in Table 2. These values are taken in part from Holdsworth et al.[8] The layers referred to in Table 2 are shown in Fig. 9 and are coincident with the hydrologic units.

TABLE 2. Important material transport properties of the five layers that remain constant in the simulations.

Layer number	Approx. horizontal groundwater velocity, m/y	Approx. vertical groundwater velocity, m/y	Longitudinal dispersion, m	Lateral dispersion, m	Molecular diffusion, m^2/y	Tortuosity
1	1.3	0.0001	50	5	10^{-5}	1.1
2	0.13	0.007	30	5	10^{-5}	1.1
3	0.008	0.001	30	10	10^{-5}	1.1
4	0.13	0.007	30	5	10^{-5}	1.1
5	1.3	0.01	50	5	10^{-5}	1.1

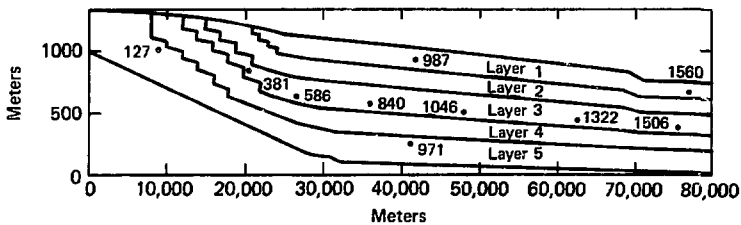

FIG. 9. A cross section of the five layers used as material property zones and the position of ten source nodes.

LOCATION OF THE SOURCE

Ten source nodes were positioned to examine the movement of material from the source in the first 5000 years of simulation, as shown in Fig. 9. Not all sources were likely sites for a nuclear waste repository, but, nevertheless, they were used to check the model calculations.

Source node 127 is located in the lower aquifer 62 km from the discharge surface. The predominant flow direction is toward the discharge region with a slight upward component. Transport from this source is rapid via both the upper and lower aquifers. Node 381 is located at the bottom of layer 3, 51 km from the discharge surface. Material movement to the phreatic surface is rapid from node 381. Source node 586 is near the bottom of layer 3, 43.25 km from the discharge surface. The ground-water flow direction at this source is about 60^{o} upward from the horizontal, toward the discharge surface. The

steady-state flow rate at node 586 is about 0.16 m/y. Material migration from this source is slower than from the two upgradient sources. Source node 840 is also located in layer 3, but is 35.25 km from the discharge surface. The ground-water flow direction at this site is 3^{0} upward from the horizontal flowing toward the discharge region. The flow rate is about 6 mm/y, and transport is minimal. Of the ten sources, node 840 is positioned best to minimize material transport because in this section of the basin the equipotential lines are parallel and nearly vertical. Source nodes 971 and 987 are located in the lower and upper aquifers, respectively, 30 km from the discharge surface. These are positioned to study the transport behavior in faster flowing (1.3 m/y) regions of the mesh. The transport from sources 1046 and 1322 is similar to that of node 840 because the three are located in the same layer in similar flow regimes. Although transport is minimal from nodes 1046 and 1322, their proximity to the discharge surface, 24 km and 8 km, respectively, makes them less suitable if one is trying to maximize breakthrough time. Source nodes 1506 and 1560 are located under the discharge surface. Node 1506 is positioned near the bottom of layer 3 and node 1560 near the bottom of the upper aquifer. These sources are used to study the transport phenomena at the downgradient end of the mesh where flow vectors are nearly vertical.

In summary, nodes 586 and 840 have the best locations for the purpose of maximizing breakthrough time. This statement is based on short-term simulations used to study the onset of transport. Source nodes 586 and 840 received additional study because of their long distance from the discharge surface and minimal transport in the first 5000 y of simulation.

SUMMARY OF MATERIAL TRANSPORT SIMULATIONS

Material transport simulations were carried out using nodes 586 and 840 as sources. The purpose was to examine the performance of the two sites by varying porosities and distribution coefficients in the layers 1 through 5 (Fig. 9).

Porosity was varied, because it can be measured directly, under field conditions by electrical geophysical methods.[9,10] Since we have some knowledge of the effective porosity at a specific site, a prediction of the

impact on model performance when porosity is varied is desirable. One-dimensional calculations can be made quickly to assess the importance of porosity, but in layered media only a computer code is practical. We have predicted the effects of porosity in such a case by multiple simulations. These calculations are subject to the assumptions previously described. Tables 3 and 4, in conjunction with Fig. 9, describe 14 simulations that were carried out twice: (1) using node 586 as the source and (2) using node 840 as the source (identified by an "a" after the run number). In these simulations, distribution coefficients in all layers are held at zero. The results from these simulations are reported in terms of average breakthrough time at the discharge surface and standard deviation of the breakthrough curve.

Results of Simulations 1-14

- Node 586 is 8 km further from the discharge surface than node 840. However, in more than half of the simulations, the average breakthrough time from source 586 is less than that from source 840. This occurs because the upward hydraulic head present at node 586 forces material sooner into the faster flowing upper aquifer.
- In the base cases (simulations 1 and 1a), the average breakthrough time from source 586 is less than that from source 840. When the porosities of the aquifers are decreased (simulations 2 and 2a), the mean arrival time at the discharge surface from both sources decreases. This occurs because material from source 586 is in the upper aquifer for most of its path to the discharge surface. When the porosities of the aquifers are increased (simulations 3 and 3a), the reverse of simulations 2 and 2a takes place; i.e., the mean arrival time at the discharge surface increases.
- In simulations 4 and 4a, the porosities in layers 2 and 4 increase. The results are increases in mean arrival times. The delay of material crossing the discharge surface from source 840 is enhanced by the absence of artesian conditions in the vicinity of node 840. By decreasing the porosities in layers 2 and 4 (simulations 5, 5a, 6, 6a, 7, 7a, 8, and 8a), mean arrival times decrease. Arrival time from source 840 is consistently slower. Using nodes 586 and 840 as sources, the model is not sensitive to porosity variations in layers 2 and 4 below 10^{-3}.

TABLE 3. Porosity values of the five layers for simulations 1 through 14.

Layer number	Simulation number													
	1	2	3	4	5	6	7	8	9	10	11	12	13	14
1	.1	.02	.2	.1	.1	.1	.1	.1	.1	.1	.1	.1	.1	.1
2	.05	.05	.05	.1	.01	10^{-3}	10^{-4}	10^{-5}	.05	.05	.05	.05	.05	.05
3	.05	.05	.05	.05	.0	.05	.05	.05	.1	.01	10^{-3}	10^{-4}	10^{-5}	10^{-6}
4	.05	.05	.05	.1	.01	10^{-3}	10^{-4}	10^{-5}	.05	.05	.05	.05	.05	.05
5	.1	.02	.2	.1	.1	.1	.1	.1	.1	.1	.1	.1	.1	.1

TABLE 4. The average breakthrough time and standard deviation of the breakthrough curves for simulations 1 through 14 (source at node 586) and simulations 1a through 14a (source at node 840).

Simulation number for node 586	Average breakthrough time, y	Standard deviation, y	Simulation number for node 840	Average breakthrough time, y	Standard deviation, y
1	5271	1283	1a	5486	1413
2	4677	1322	2a	5052	1461
3	5909	1193	3a	5671	1228
4	5661	1470	4a	5871	1495
5	4914	1111	5a	5145	1349
6	4831	1075	6a	5066	1338
7	4823	1072	7a	5059	1337
8	4822	1071	8a	5058	1337
9	5369	1333	9a	5829	1564
10	5163	1222	10a	5119	1250
11	5127	1206	11a	5028	1215
12	5122	1204	12a	5019	1212
13	5122	1204	13a	5018	1211
14	5122	1204	14a	5018	1211

- The porosity of layer 3 is increased for simulations 9 and 9a. In both cases, average breakthrough times increase. Material from source 840 has a longer resident time in layer 3 than material from 586. The resident time of material from 840 is extended significantly by increasing porosity. Decreasing the porosity of layer 3 forces material to move faster away from the source. As a result, the mean arrival time decreases (simulations 10, 10a, 11, 11a, 12, 12a, 13, 13a, 14, and 14a). The quicker that material leaves layer 3 at both sites, the more attractive node 586 becomes as a repository location. When the porosity in layer 3 is low, the main barrier to breakthrough is the travel distance in the upper aquifer. The model is not sensitive to porosity variations, in layer 3, below 10^{-3} when either node 586 or node 840 is the source.

Results of Simulations 15-21

The distribution coefficients in layers 1 through 5 were varied, while the porosities of layers 1 through 5 were held at 0.1, 0.05, 0.01, 0.05, and 0.1, respectively. Distribution coefficients were varied because the present state of knowledge of this parameter is in its infancy.[11] The impact of the distribution coefficient on the model's performance allows us to assess the importance of the parameter, at least relative to porosity. Table 5 describes seven simulations (15-21), each of which was then performed twice: (1) using node 586 as the source and (2) using node 840 as the source. The results from these simulations were analyzed in terms of initial breakthrough time at the discharge surface. This was necessary because the maximum simulation time was 250,000 years, which was insufficient time in some runs to calculate accurately the mean arrival time. The results can be summarized as follows:

- Simulations 15 and 15a are the base cases using nodes 586 and 840, respectively, as source nodes. The initial breakthrough for these runs is at about 2300 y, with 15a being somewhat earlier. By setting the distribution coefficient to 10.0 in all layers, the initial breakthrough comes at 100,000 y in simulation 16 and at 85,000 y in 16a. In simulations 17 and 17a, the distribution coefficient equals 100.0 throughout the mesh. The result is no breakthrough after 250,000 y of simulation.

- In simulations 18 and 18a, layer 3 has a K_d of 10.0, while in the other layers it is set to 0.0. The initial breakthrough times increase only slightly from the base case because most of the travel-path length of the material is in layers 1 and 2. Similarly, in runs 19 and 19a, only a small increase in initial breakthrough occurs.
- The distribution coefficients (K_d) in the aquifers are increased to 10.0 (runs 20 and 20a) and 100.0 (runs 21 and 21a) and set at 0.0 in the other layers in order to single out the effect from the aquifer. The effect from the aquifer K_d, by itself, is an initial breakthrough of 38,000 y for run 20, 13,000 y for run 20a, and no breakthrough in 250,000 y for runs 21 and 21a. Clearly, the K_d of the upper aquifer is the most important parameter controlling transport in this study.

TABLE 5. Distribution coefficients (ml/g) of the five layers for simulations 15 through 21.

Layer number	Simulation number						
	15	16	17	18	19	20	21
1	0	10	100	0	0	10	100
2	0	10	100	0	0	0	0
3	0	10	100	10	100	0	0
4	0	10	100	0	0	0	0
5	0	10	100	0	0	10	100

RECOMMENDATIONS

Based on the design and assumptions of this model, it has been possible to make statements about the influence of porosity and distribution coefficient on long-term material transport simulations. The results of this study lean heavily on the assumptions set forth at the beginning of this report; they should be interpreted with care. Future modeling efforts should be aimed at reducing the number of assumptions. Such models could include three-dimensional flow and transient flow capabilities.

One might also consider a wider range of:

- water table configurations
- geological configurations
- parameter values.

If the modeling techniques used in this study were applied to a field situation in order to predict transport, the uncertainty in the field measurements themselves, in addition to the uncertainty caused by extrapolating the measurements over a large area, would more than likely mask the correct conclusion. We therefore recommend two concurrent tasks:

- An evaluation of the necessity for more complex models to simulate regional ground-water flow and material transport
- A review of the geotechnical measurement and model parameter uncertainties inherent in regional ground-water and material transport models.

ACKNOWLEDGEMENTS

The authors particularly wish to thank G. D. Mendez for his programming support during this study. Suggestions from R. Stone and R. A. Freeze in preparing the manuscript are also appreciated.

REFERENCES

1. J. F. Pickens and W. C. Lennox, "Numerical Simulation of Waste Movement in Steady Groundwater Flow Systems," Water Resources Research 12, (2) pp. 171-180 (1976).
2. F. W. Schwartz, "On Radioactive Waste Management: An Analysis of the Parameters Controlling Subsurface Contaminant Transfer," J. of Hydrology 27, pp. 51-71 (1975).
3. R. L. Taylor and C. B. Brown, "Darcy Flow Solutions with a Free Surface," Proceedings, American Society of Civil Engineers, Journal of Hydraulics Division 93 (HY2), pp. 25-33 (1967).
4. T. G. Naymik, User's Manual for a Two-Dimensional Ground-Water Flow Code on the Octopus Computer Network, Lawrence Livermore Laboratory, Livermore, CA, UCID-17908 (1978).
5. J. O. Duguid and M. Reeves, Material Transport Through Porous Media: A Finite-Element Galeskin Model, Oak Ridge National Laboratory, Oak Ridge, TN, ORNL-4928, Environmental Sciences Division Publication 733, p. 201 (1976).
6. T. G. Naymik and G. D. Mendez, User's Manual for a Material Transport Code on the Octopus Computer Network, Lawrence Livermore Laboratory, Livermore, CA, UCID-17986 (1978).
7. J. Bear, Dynamics of Fluids in Porous Media (American Elsevier Publishing Co. Inc., New York, 1971).
8. T. Holdsworth, D. Towse, D. J. Isherwood, T. F. Harvey, and R. A. Heckman, High-Level Waste Repository Site Suitability Study--Interim Report, Lawrence Livermore Laboratory, Livermore, CA, UCID-17879 (1978).
9. G. V. Keller and F. C. Frischknecht, Electrical Methods in Geophysical Prospecting (Pergamon Press, 1966).
10. J. R. Wait, Electromagnetic Probing in Geophysics (The Golem Press, Boulder, CO, 1971).

11. I. Y. Borg, R. Stone, H. B. Levy, and L. D. Ramspott, Information Pertinent to the Migration of Radionuclides in Groundwater at the Nevada Test Site, Lawrence Livermore Laboratory, Livermore, CA, UCRL-52078 (1976).

PS/n11